Natural Resources for Human Health
eISSN: 2583-1194

Original Research

Received 25 May 2026
Revised 29 June 2026
Accepted 17 July 2026

Natural Resources for Human Health 2026, Vol. 6 (9s): 953–964

KEYWORDS:
Ovarian cancer; Biofabricated nanoparticles; Selenium nanoparticles; Silver nanoparticles; Sinapis nigra; Nanomedicine; Nanotherapeutics

Comparative Evaluation of Sinapis nigra-Derived Selenium and Silver Nanoparticles: Physicochemical Characterization, Antioxidant Activity and Anticancer Responses in Ovarian Cancer Cells

Srilakshmi Samanchi[1]*, P. Josthna[1], G. Sai Sri Rekha[2]

[1]*Research Scholar, Department of Biotechnology, Sri Padmavathi Mahila Viswavidyalayam, Tirupati, India,
*Corresponding author: email: (srilak.01@gmail.com)
[1]Professor, Department of Biotechnology, Sri Padmavathi Mahila Viswavidyalayam, Tirupati, India
[2]Professor, Department of Biotechnology, Andhra Loyola College (Autonomous), Vijayawada, India

ABSTRACT: Ovarian cancer remains a clinically challenging gynecological malignancy because many patients present with advanced disease and recurrent tumors may develop treatment resistance. Plant-mediated nanoparticle fabrication provides a route for generating multifunctional nanomaterials in which the inorganic core is associated with biologically active surface constituents. In the present study, selenium nanoparticles (MS-SeNPs) and silver nanoparticles (MS-AgNPs) were biofabricated using aqueous Sinapis nigra seed extract as a reducing, capping and stabilizing system, with ascorbic acid incorporated as an auxiliary reducing and stabilizing component. Successful formation was indicated by characteristic colour changes and supported by UV–Visible, FTIR, dynamic light scattering (DLS), zeta-potential and X-ray diffraction (XRD) analyses. MS-SeNPs displayed an absorption maximum at 262 nm, whereas MS-AgNPs showed a prominent surface-plasmon band at 427 nm. FTIR spectra indicated the contribution of hydroxyl, carbonyl, amide and sulfur-associated biomolecular groups to nanoparticle surface chemistry. MS-SeNPs exhibited a mean zeta potential of −69.9 mV, while MS-AgNPs showed +30.3 mV. XRD patterns were consistent with semicrystalline hexagonal selenium for MS-SeNPs and crystalline face-centered cubic silver for MS-AgNPs. Both nanoparticle systems demonstrated concentration-dependent DPPH, hydrogen-peroxide and nitric-oxide scavenging activities, with maximum responses of approximately 75%, 70% and 68%, respectively, for MS-SeNPs and approximately 74%, 68% and 64% for MS-AgNPs. In TOV112D ovarian cancer cells, both materials produced concentration-dependent cytotoxicity. MS-SeNPs showed an IC_{50} of 32.76 µg/mL compared with 58.81 µg/mL for MS-AgNPs. Scratch assays further indicated stronger inhibition of cell migration by MS-SeNPs, while intracellular DCFH-DA fluorescence increased following nanoparticle exposure, suggesting altered cellular redox homeostasis. Taken together, the results indicate that plant-mediated MS-SeNPs and MS-AgNPs possess multifunctional biological activity, with MS-SeNPs showing comparatively stronger cytotoxic, anti-migratory and redox-modulating responses under the conditions tested. These findings support further investigation of biofabricated SeNPs as experimental nanotherapeutic candidates for ovarian cancer. However, the present evidence remains preclinical and in vitro; selectivity toward non-malignant cells,

Natural Resources for Human Health
eISSN: 2583-1194

molecular mechanisms, pharmacokinetics, biodistribution, dose optimization and in vivo safety require systematic evaluation before translational consideration.

1. INTRODUCTION

Ovarian cancer comprises a heterogeneous group of malignancies with distinct histological, molecular and clinical characteristics. Epithelial ovarian cancer accounts for most clinically relevant cases, and diagnosis frequently occurs at an advanced stage. Current management combines cytoreductive surgery with platinum-based chemotherapy, while treatment selection is increasingly influenced by molecular features and previous treatment response. Despite substantial therapeutic progress, recurrent disease and acquired resistance remain major barriers to durable disease control [1–4]. Contemporary guidelines incorporate platinum-based combinations, maintenance strategies, targeted approaches and biomarker-directed treatments, illustrating both the expanding therapeutic armamentarium and the continuing need for approaches that can address treatment resistance and disease heterogeneity [4,5].

Oxidative stress is particularly relevant to ovarian-cancer biology. Reactive oxygen species (ROS) participate in proliferation, DNA damage, metabolic adaptation, signalling and tumour–stroma interactions. Malignant cells can nevertheless adapt to elevated basal ROS by increasing antioxidant capacity, creating a narrow redox range in which additional oxidative stress may become cytotoxic [6,7]. This concept has stimulated interest in nanomaterials capable of modifying intracellular redox balance while simultaneously influencing other biological processes.

Nanoparticles provide a versatile platform because their physicochemical behaviour can be altered through particle size, morphology, crystallinity, surface charge and surface-associated biomolecules. These parameters affect colloidal stability, protein adsorption, cellular interactions and intracellular trafficking [8–11]. Dynamic light scattering and zeta-potential measurements therefore provide complementary information on hydrodynamic behaviour and surface electrostatics, whereas XRD, FTIR and UV–Visible spectroscopy provide information on crystallinity, surface chemistry and optical properties, respectively [9–12].

Selenium is an essential trace element involved in selenoprotein-dependent redox regulation and other physiological processes. Elemental selenium nanoparticles have attracted attention because nanoscale selenium can display biological properties distinct from conventional selenium compounds, while offering opportunities for surface functionalization and drug or biomolecule delivery [13–18,37]. Plant-mediated fabrication is particularly attractive because plant metabolites can participate in reduction and stabilization, producing a biologically coated nanoparticle surface rather than an unfunctionalized inorganic interface [15–18].

Silver nanoparticles represent a useful comparator because silver has established antimicrobial activity and AgNPs have also been investigated for anticancer applications. Their biological effects can involve oxidative stress, mitochondrial perturbation, membrane interactions and DNA damage, although these responses are strongly dependent on size, dose, surface chemistry and experimental context [19–22]. Direct comparison of biofabricated SeNPs and AgNPs generated using the same botanical matrix can therefore help distinguish effects associated with the elemental core from those contributed by a common phytochemical environment.

Sinapis nigra (black mustard) contains glucosinolates and other sulfur-containing and phenolic constituents that provide a chemically active plant matrix [23,24]. Such metabolites are plausible contributors to the reduction and stabilization of metal or metalloid nanoparticles. The present work consequently evaluated MS-SeNPs and MS-AgNPs prepared from S. nigra seed extract and compared their physicochemical properties, cell-free antioxidant activity and anticancer-associated responses in the TOV112D ovarian cancer cell line. The experimental workflow was designed to connect nanoparticle formation and surface characteristics with cytotoxicity, migration inhibition and intracellular ROS generation.

2. MATERIALS AND METHODS

2.1. Plant material and chemicals

Sinapis nigra seeds were collected from local fields in Tirupati, Andhra Pradesh, India. Sodium selenite (Na_2SeO_3), silver nitrate ($AgNO_3$), ascorbic acid, DPPH, hydrogen peroxide, sodium nitroprusside, Griess reagent, MTT and DCFH-based

reagents were used as described in the experimental protocol. Antibiotic discs were obtained from HiMedia and laboratory glassware from Borosil. The TOV112D ovarian cancer cell line was used for the in vitro anticancer experiments.

2.2. Preparation of Sinapis nigra seed extract

Seeds were cleaned, shade-dried at room temperature and finely powdered. Five grams of seed powder were suspended in 100 mL distilled water, adjusted to approximately pH 7.0 and boiled for 15 min. The extract was filtered through Whatman No. 1 filter paper and stored under refrigerated conditions until use.

2.3. Biofabrication of MS-SeNPs and MS-AgNPs

Fresh S. nigra aqueous extract was added dropwise under continuous magnetic stirring to separate reaction mixtures containing 1 mL of 10 mM sodium selenite and silver nitrate, respectively. The mixtures were maintained in the dark at 27 ± 2 °C with continuous agitation at 120 rpm for 24 h. Ascorbic acid was incorporated as an auxiliary reducing and stabilizing component. Formation of MS-SeNPs was accompanied by a pale-yellow to brick-red colour transition, whereas the silver reaction mixture changed from pale yellowish-white to black. After reaction completion, nanoparticles were recovered by high-speed centrifugation, washed repeatedly with sterile distilled water and suitable organic solvents, and finally resuspended in sterile Milli-Q water. Samples were stored under refrigerated, light-protected conditions until characterization and biological evaluation.

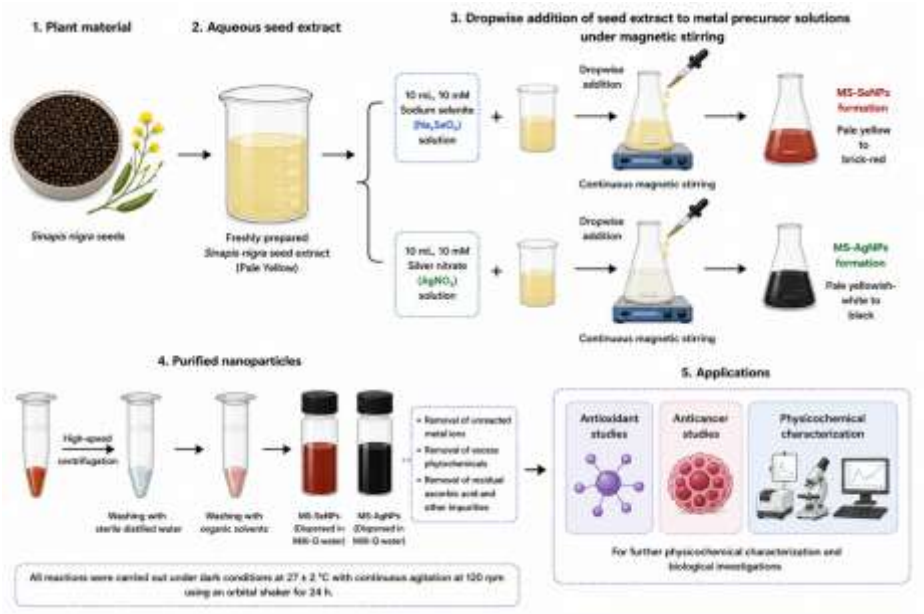

Figure 1. Schematic workflow for plant-mediated biofabrication of MS-SeNPs and MS-AgNPs using Sinapis nigra seed extract. The original experimental schematic is retained from the supplied manuscript.

2.4. Physicochemical characterization

UV–Visible spectra were recorded over 220–750 nm. FTIR spectroscopy was used to examine functional groups associated with the nanoparticle surface. DLS/particle-size analysis was used to assess hydrodynamic size and distribution, while zeta-potential analysis was used to evaluate surface charge and colloidal behaviour. XRD was used to assess crystallographic structure and phase characteristics. These methods were interpreted together because no single measurement describes the complete physicochemical identity of a plant-mediated nanoparticle [9–12].

2.5. In vitro antioxidant assays

Antioxidant activity was assessed by DPPH, hydrogen-peroxide and nitric-oxide scavenging assays using ascorbic acid as the reference antioxidant. DPPH scavenging was monitored at 517 nm following incubation in the dark. Hydrogen-peroxide scavenging was evaluated at 230 nm. For nitric-oxide scavenging, sodium nitroprusside was used as the NO donor and the generated nitrite was quantified using Griess reagent at 546 nm. Concentration-dependent inhibition curves were used to

estimate antioxidant responses. The DPPH assay follows the established radical-reduction principle described by Brand-Williams et al. [25].

2.6. In vitro cytotoxicity assay

TOV112D ovarian cancer cells were exposed to increasing concentrations of MS-SeNPs or MS-AgNPs and cell viability was evaluated by the MTT colorimetric assay. Percentage inhibition and IC_{50} values were derived from concentration–response profiles. The assay is based on the reduction of tetrazolium salt by metabolically active cells [26].

2.7. Scratch migration assay

A cell-free gap was generated in confluent TOV112D monolayers and images were recorded at 0 and 24 h following nanoparticle exposure. Wound closure was calculated relative to the initial wound area. Because scratch closure can reflect both migration and proliferation, the results are interpreted here as an anti-migratory-associated response rather than definitive proof of inhibition of migration alone.

2.8. Intracellular ROS assay

Intracellular ROS-associated fluorescence was assessed using a DCFH-DA-based assay following nanoparticle treatment. Hydrogen peroxide served as a positive oxidative-stress control. DCF-based fluorescence is widely used as a general oxidative-stress indicator, but it is not specific for a single ROS species and should therefore be interpreted as ROS-associated oxidative activity rather than direct identification of a particular radical [27,28].

3. Results and Discussion

3.1. Optical confirmation of nanoparticle formation

The UV–Visible spectra provided an initial optical indication of nanoparticle formation. MS-SeNPs showed a characteristic absorption maximum at 262 nm, accompanied by the experimentally observed pale-yellow to brick-red colour transition. MS-AgNPs exhibited a prominent band at 427 nm with slight broadening toward the longer-wavelength region, consistent with localized surface-plasmon resonance of silver nanoparticles. Plant-mediated nanoparticle synthesis commonly produces optical responses that depend on core composition, particle size, morphology and the chemical environment of surface-bound metabolites [15,19,20]. The difference between the selenium and silver spectra therefore reflects the distinct electronic properties of the two elemental systems rather than a difference in the botanical reducing matrix alone.

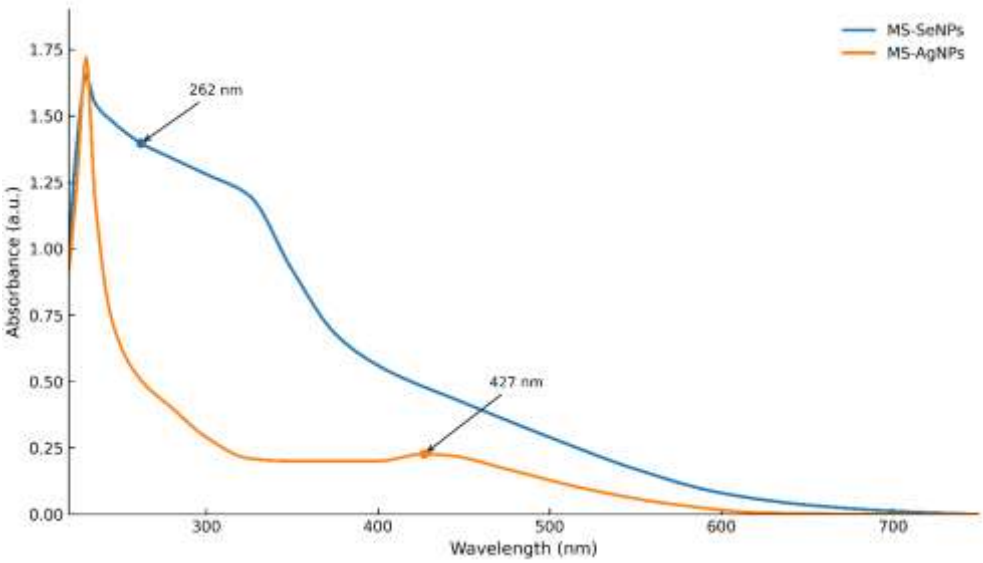

Figure 2. UV–Visible spectra of biofabricated MS-SeNPs and MS-AgNPs. The principal absorption maxima were observed at 262 nm and 427 nm, respectively.

3.2. FTIR evidence for phytochemical-associated surface chemistry

Both nanoparticle systems displayed FTIR bands associated with hydroxyl/amine, carbonyl/amide and lower-frequency sulfur-associated vibrations. A broad band centred around 3343 cm^{-1} was consistent with O–H/N–H stretching, while the band near 1636 cm^{-1} was attributed primarily to amide-I carbonyl stretching and/or conjugated C=C-associated vibrations. A lower-frequency feature around 635.99 cm^{-1} was observed in the nanoparticle spectra. The overall spectral pattern supports the participation of seed-derived biomolecules in nanoparticle formation and surface association. This interpretation is consistent with the established role of plant phenolics, proteins and sulfur-containing metabolites in reduction and stabilization during biological nanoparticle fabrication [15,18,23,24]. FTIR alone, however, cannot establish the exact identity of each surface-bound molecule; complementary chromatographic or mass-spectrometric profiling would be required for molecular assignment.

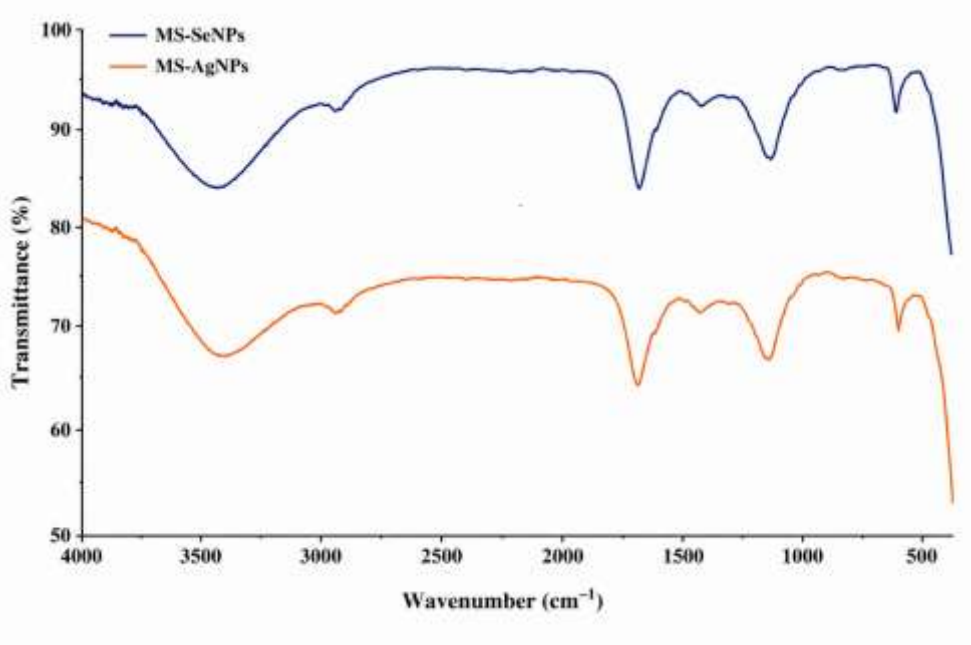

Figure 3. FTIR spectra of biofabricated MS-SeNPs and MS-AgNPs, showing shared and nanoparticle-specific bands associated with phytochemical surface functionalization.

3.3. Particle size, surface charge and crystallographic characteristics

DLS analysis confirmed nanoscale hydrodynamic behaviour for the two formulations. The supplied analysis reported a Z-average hydrodynamic diameter of 14.4 nm and a PDI of 0.209 for MS-AgNPs. MS-SeNPs were also described as nanoscale, with moderate distributional heterogeneity consistent with the chemically diverse surface environment expected from plant-mediated synthesis. DLS measures hydrodynamic diameter rather than the inorganic core diameter, and its output can be influenced by surface-associated biomolecules, aggregates and concentration; accordingly, DLS values should not be treated as interchangeable with crystallite or microscopy-based particle dimensions [9,10,29].

MS-SeNPs exhibited a mean zeta potential of −69.9 mV, with two charge populations centred at approximately −30.9 and −116.1 mV, whereas MS-AgNPs showed a single positive population centred at +30.3 mV. These values indicate substantially different interfacial electrostatic environments despite the common plant-derived synthesis matrix. The high absolute charge of MS-SeNPs is compatible with strong electrostatic repulsion, while the AgNP value lies around the commonly used threshold associated with electrostatic colloidal stability [30]. Nevertheless, zeta potential is influenced by pH, ionic strength, measurement medium and electrokinetic modelling; it should therefore be considered one component of stability assessment rather than a standalone proof of long-term storage stability [30,31].

Natural Resources for Human Health
eISSN: 2583-1194

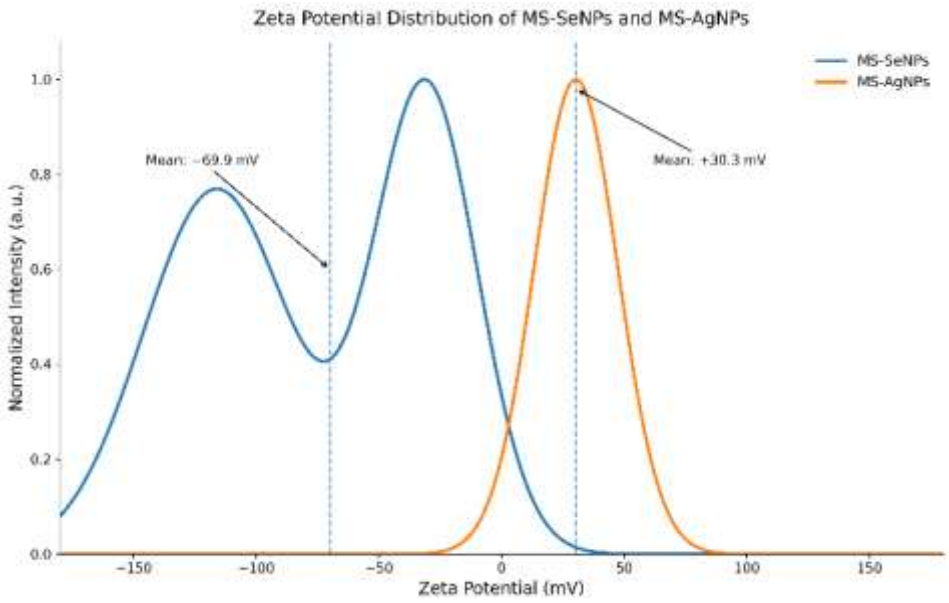

Figure 4. Zeta-potential distributions of MS-SeNPs and MS-AgNPs, showing the contrasting negative and positive surface-charge profiles.

XRD analysis further differentiated the two nanoparticle systems. MS-SeNPs displayed reflections at 23.34°, 29.70°, 31.92°, 43.65°, 45.40° and 51.72°, consistent with hexagonal selenium according to the phase assignment reported in the supplied manuscript. The broad diffuse contribution between approximately 15° and 35° suggested a semicrystalline–amorphous component, plausibly associated with phytochemical material surrounding the selenium phase. MS-AgNPs showed reflections at 38.12°, 44.28°, 64.46° and 77.41°, assigned to the (111), (200), (220) and (311) planes of face-centered cubic silver. These observations support a more highly crystalline AgNP core compared with the partially amorphous phytochemical-associated MS-SeNP system. Crystallite dimensions inferred from XRD should be regarded as coherent diffraction-domain dimensions rather than direct measurements of the complete particle diameter [32].

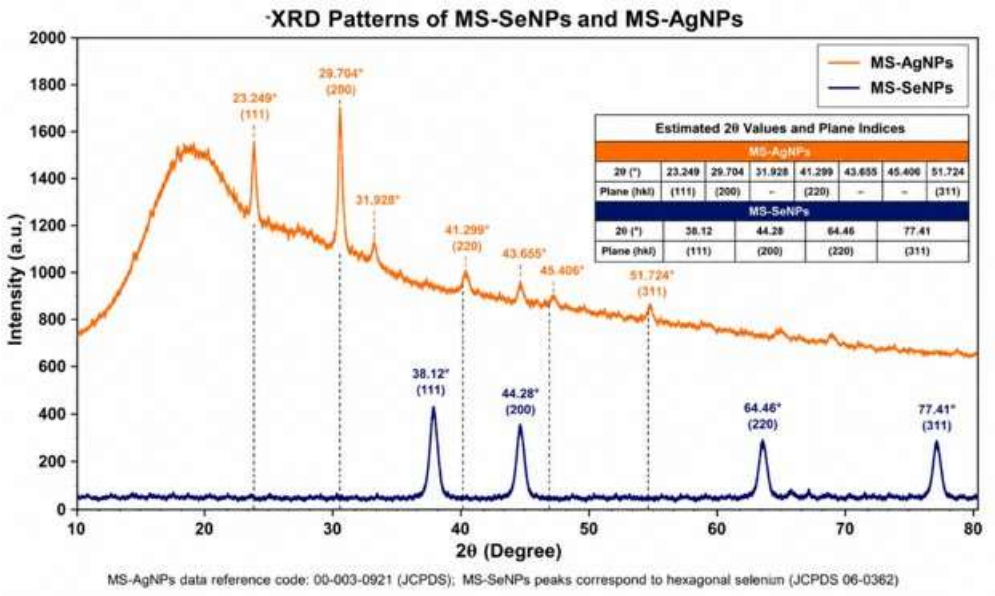

Figure 5. XRD patterns of MS-SeNPs and MS-AgNPs. The selenium pattern shows multiple reflections with a broad diffuse contribution, whereas the silver pattern displays characteristic face-centered cubic reflections.

Natural Resources for Human Health
eISSN: 2583-1194

3.4. In vitro antioxidant activity

Both formulations showed concentration-dependent scavenging of DPPH, hydrogen peroxide and nitric oxide, indicating measurable cell-free radical-neutralizing capacity. In the DPPH assay, MS-SeNPs reached approximately 75% inhibition at the highest tested concentration, compared with approximately 74% for MS-AgNPs. Hydrogen-peroxide scavenging reached approximately 70% for MS-SeNPs and 68% for MS-AgNPs, while nitric-oxide scavenging reached approximately 68% and 64%, respectively. DPPH responses are influenced by hydrogen- or electron-transfer reactions, whereas the hydrogen-peroxide and nitric-oxide assays probe different chemical environments; therefore, the agreement across assays provides stronger evidence of broad cell-free redox activity than reliance on a single antioxidant assay [25,33].

The modestly higher scavenging responses of MS-SeNPs may reflect the combined contribution of elemental selenium and the phytochemical corona produced during biofabrication. However, the present assays cannot separate the contribution of the inorganic core from that of residual or surface-bound seed constituents. Moreover, cell-free antioxidant activity should not be equated directly with intracellular antioxidant protection. Nanoparticles can undergo protein adsorption, aggregation, cellular uptake and intracellular transformation, creating biological conditions that differ substantially from simple acellular radical-scavenging systems [34–36].

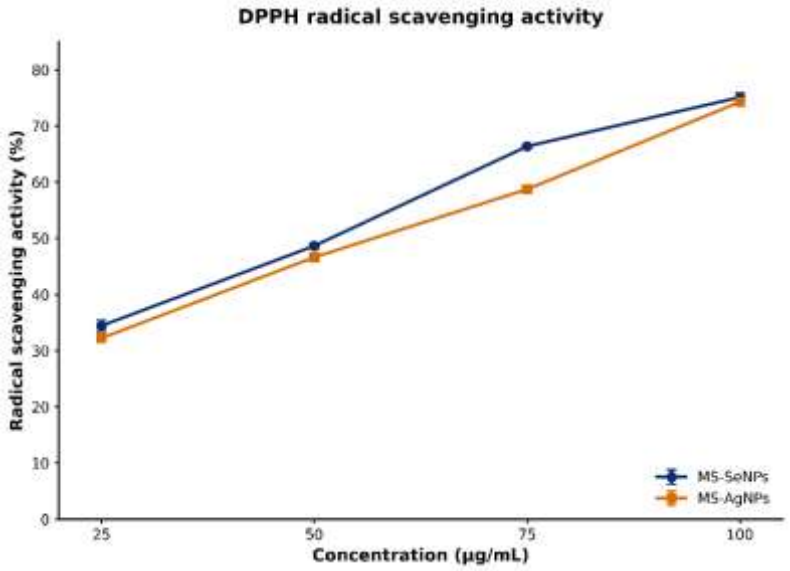

Figure 6. DPPH radical-scavenging activity of MS-SeNPs and MS-AgNPs across the tested concentration range.

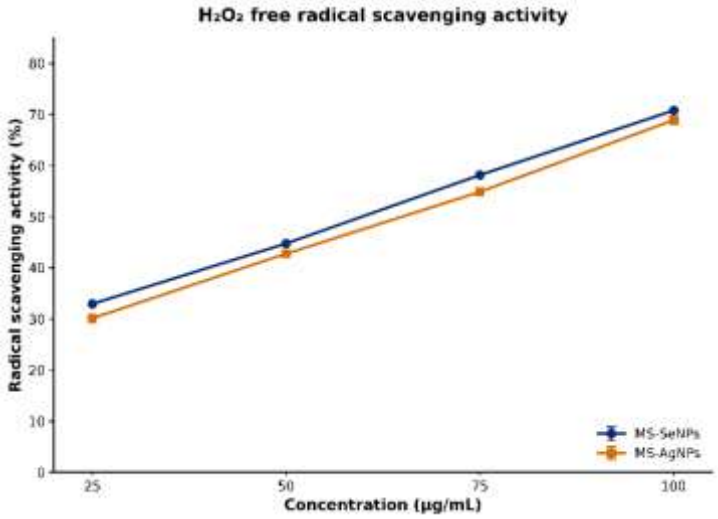

Figure 7. Hydrogen-peroxide scavenging activity of MS-SeNPs and MS-AgNPs across the tested concentration range.

Natural Resources for Human Health
eISSN: 2583-1194

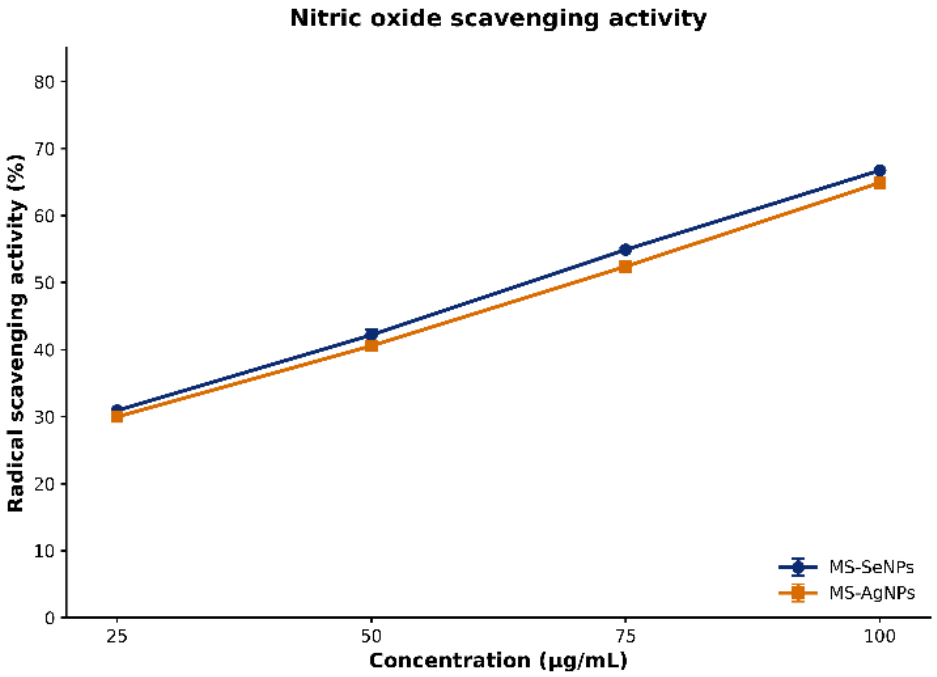

Figure 8. Nitric-oxide scavenging activity of MS-SeNPs and MS-AgNPs across the tested concentration range.

3.5. Cytotoxicity against TOV112D ovarian cancer cells

Both nanoparticle systems produced concentration-dependent inhibition of TOV112D cell viability. MS-AgNP-mediated inhibition increased from 12.87% at 10 µg/mL to 73.68% at 100 µg/mL, yielding an IC_{50} of 58.81 µg/mL. MS-SeNPs produced 15.56% inhibition at 5 µg/mL and increased to 77.41% at 80 µg/mL, with an IC_{50} of 32.76 µg/mL. Under the conditions used, the lower IC_{50} of MS-SeNPs indicates greater apparent cytotoxic potency than MS-AgNPs.

This difference is biologically plausible because SeNP and AgNP systems can interact differently with cellular membranes, proteins and intracellular redox pathways. Published work has linked SeNP exposure to ROS modulation, mitochondrial dysfunction and programmed-cell-death pathways, while AgNP responses have also been associated with oxidative stress, DNA damage and mitochondrial perturbation [13,19,21,22,37]. Nevertheless, an MTT-derived IC_{50} is a measure of metabolic viability and does not by itself establish a specific cell-death pathway. The observed difference between MS-SeNPs and MS-AgNPs should therefore be considered a comparative in vitro potency finding rather than evidence of selective tumour-cell toxicity.

3.6. Anti-migratory-associated response in the scratch assay

Untreated TOV112D monolayers showed approximately 50–54% wound closure after 24 h. MS-SeNP exposure reduced wound closure to 12.01–15.09% at 5 µg/mL and 9.00–10.84% at 10 µg/mL, corresponding to approximately 85–91% residual wound area. MS-AgNPs produced 18.96–22.67% closure at 10 µg/mL and 16.97–19.44% at 20 µg/mL, leaving approximately 77–83% residual wound area. Thus, MS-SeNPs produced the stronger suppression of wound closure under the tested conditions.

Reduced wound closure may be relevant to the invasive phenotype of ovarian cancer, but scratch assays cannot distinguish migration from changes in proliferation or cell survival unless appropriate controls are incorporated. The stronger effect observed for MS-SeNPs is therefore best described as inhibition of wound closure or an anti-migratory-associated response. Future experiments incorporating mitomycin-controlled migration assays, transwell migration/invasion models and EMT-associated markers would help determine whether the response reflects a direct effect on migratory signalling [3,39].

3.7. Intracellular ROS generation

The DCFH-DA assay showed concentration-associated increases in ROS-related fluorescence following nanoparticle exposure, with hydrogen peroxide producing the expected strong positive response. This observation provides a mechanistic link between nanoparticle exposure and altered cellular redox state. The finding is also consistent with the lower MS-SeNP IC_{50} and the stronger suppression of wound closure observed in the functional assays. In ovarian cancer, elevated basal oxidative stress and increased dependence on antioxidant systems can create a therapeutic vulnerability when additional oxidative burden exceeds cellular buffering capacity [6,7].

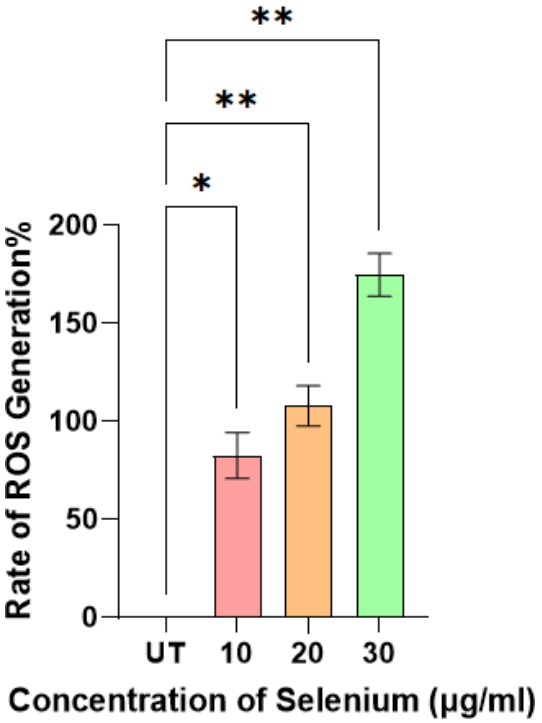

Figure 9. Intracellular ROS-associated fluorescence following exposure of TOV112D cells to the tested selenium concentrations.

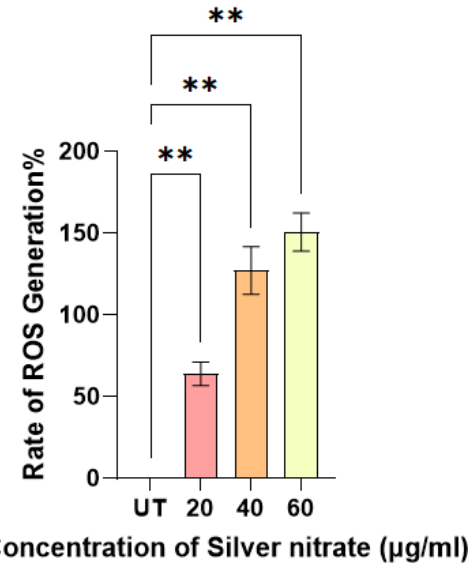

Figure 10. Intracellular ROS-associated fluorescence following exposure of TOV112D cells to the tested silver concentrations.

The apparent coexistence of cell-free antioxidant activity and intracellular ROS generation is not necessarily contradictory. In an acellular assay, surface-associated phytochemicals may directly quench model radicals. In cells, nanoparticles encounter proteins, membranes, organelles and redox-active compartments, and their uptake or transformation can produce a different net biological response. Protein-corona formation and changes in nanoparticle surface identity can further modify cellular uptake and intracellular fate [34–36]. Importantly, DCFH-DA is a general oxidative-stress probe with recognized specificity limitations; the fluorescence signal should therefore not be interpreted as direct evidence for one specific ROS species [27,28].

3.8. Integrated interpretation and translational significance

Taken together, the characterization and biological results indicate that the two nanoparticles are not functionally interchangeable, even though they were fabricated using the same S. nigra seed matrix. MS-SeNPs combined a strongly negative surface potential with a semicrystalline selenium phase and phytochemical-associated surface chemistry, whereas MS-AgNPs displayed a positive surface potential and a more highly crystalline metallic silver phase. These physicochemical differences provide a reasonable basis for the observed divergence in biological behaviour, although causal relationships between any single physicochemical parameter and biological activity cannot be established from the present dataset alone [9–12].

The stronger in vitro cytotoxic and wound-closure-inhibitory responses of MS-SeNPs, together with increased intracellular ROS-associated fluorescence, support further investigation of this formulation as an experimental ovarian-cancer nanotherapeutic candidate. Selenium nanomaterials are increasingly being investigated not only as direct cytotoxic agents but also as platforms for therapeutic cargo delivery and combination treatment [13–17,37,39]. For example, functionalized SeNP systems have been used to deliver paclitaxel and to exploit ROS-linked signalling in cancer models [39]. Such studies support the broader concept that SeNPs may act as multifunctional nanomaterials rather than simply as elemental selenium sources.

At the same time, the current evidence does not establish tumour selectivity or clinical efficacy. No non-malignant ovarian or normal epithelial comparator was included in the supplied experiments, and no animal model, pharmacokinetic analysis, biodistribution study or long-term toxicity assessment was performed. The influence of nanoparticle dose, serum protein corona, aggregation state, biological medium and batch-to-batch variation also requires systematic investigation. These issues are particularly important for plant-mediated nanoparticles because the chemical composition of the biological coating can vary with plant source, extraction conditions and reaction parameters [15,18,23,34].

A logical next stage would combine mechanistic assays with formulation standardization. Mitochondrial membrane-potential analysis, Annexin V/propidium iodide staining, caspase activation, DNA-damage markers, glutathione measurements and ROS-rescue experiments would clarify whether oxidative stress is upstream of cell death. Proteomic or metabolomic profiling of the nanoparticle corona could help define the biological identity acquired in cell culture. Finally, studies using normal cells, three-dimensional ovarian-cancer models and in vivo systems are necessary before any claim of therapeutic selectivity or translational utility can be made.

Overall Summary and Conclusion

The present study provides an integrated comparison of selenium and silver nanoparticles biofabricated using aqueous Sinapis nigra seed extract and evaluates their physicochemical and biological behaviour in the context of ovarian-cancer research. The synthesis strategy combined the reducing, capping and stabilizing capacity of the botanical extract with ascorbic acid as an auxiliary reducing and stabilizing component. The resulting materials displayed distinct optical, surface and crystallographic properties. MS-SeNPs showed an absorption maximum at 262 nm and a strongly negative mean zeta potential of −69.9 mV, whereas MS-AgNPs exhibited a characteristic surface-plasmon band at 427 nm and a positive zeta potential of +30.3 mV. FTIR findings supported the association of hydroxyl, amide, carbonyl and sulfur-containing biomolecular groups with the nanoparticle surfaces, while XRD indicated a semicrystalline selenium-containing phase for MS-SeNPs and a more highly crystalline face-centered cubic silver phase for MS-AgNPs. These observations demonstrate that the common botanical matrix produced two chemically distinct nanomaterials rather than a single generic nanoparticle phenotype.

Functionally, both formulations exhibited concentration-dependent free-radical scavenging activity against DPPH, hydrogen peroxide and nitric oxide, with MS-SeNPs showing slightly higher maximum responses in all three assays. In TOV112D ovarian cancer cells, both materials produced concentration-dependent cytotoxicity, but MS-SeNPs showed greater apparent potency, with an IC_{50} of 32.76 μg/mL compared with 58.81 μg/mL for MS-AgNPs. The scratch assay similarly

demonstrated stronger inhibition of wound closure following MS-SeNP treatment. Increased DCFH-DA-associated fluorescence after nanoparticle exposure provides evidence of altered intracellular redox status and offers a plausible mechanistic connection between nanoparticle treatment and reduced cellular viability. However, ROS generation should be interpreted as an associated mechanism rather than definitive proof of apoptosis or a specific oxidative pathway, particularly because DCFH-DA lacks species-level specificity.

An important feature of the findings is the coexistence of antioxidant activity in cell-free systems with increased intracellular ROS. This apparent dual behaviour emphasizes that nanoparticle redox effects are context dependent and influenced by surface chemistry, cellular uptake, protein corona formation, intracellular localization and dose [34–36]. The comparatively stronger responses observed with MS-SeNPs therefore warrant further investigation, but they should not yet be interpreted as evidence of clinical superiority or selective tumour toxicity. Overall, the study supports S. nigra-derived MS-SeNPs as a promising experimental nanomaterial for ovarian-cancer research, with potential relevance to redox modulation, cytotoxicity and inhibition of tumour-cell wound closure. Future work should prioritize normal-cell selectivity, mechanistic apoptosis studies, mitochondrial and DNA-damage analyses, formulation reproducibility, pharmacokinetics, biodistribution and in vivo toxicity and efficacy. Such studies will determine whether the observed in vitro activity can be developed into a reproducible and clinically relevant nanomedicine strategy.

REFERENCES

[1] Scott M, et al. Ovarian cancer. Nat Rev Dis Primers. 2026;12:9. doi:10.1038/s41572-026-00686-x.
[2] Siegel RL, Giaquinto AN, Jemal A. Cancer statistics, 2024. CA Cancer J Clin. 2024;74(1):12–49. doi:10.3322/caac.21820.
[3] Matulonis UA, Sood AK, Fallowfield L, Howitt BE, Sehouli J, Karlan BY. Ovarian cancer. Nat Rev Dis Primers. 2016;2:16061. doi:10.1038/nrdp.2016.61.
[4] Lesnock JL, Temin S, Bouberhan S, et al. Systemic Treatment of Ovarian Cancer Recurrence: ASCO Living Guideline, Version 2026.1.0. J Clin Oncol. 2026. doi:10.1200/JCO-26-01591.
[5] Tew WP, Lacchetti C, Ellis A, et al. PARP Inhibitors in the Management of Ovarian Cancer: ASCO Guideline. J Clin Oncol. 2020;38(30):3468–3493. doi:10.1200/JCO.20.01924.
[6] Saed GM, Diamond MP, Fletcher NM. Updates of the role of oxidative stress in the pathogenesis of ovarian cancer. Gynecol Oncol. 2017;145(3):595–602. doi:10.1016/j.ygyno.2017.02.033.
[7] Kobayashi H, Imanaka S, Shigetomi H. Revisiting therapeutic strategies for ovarian cancer by focusing on redox homeostasis. Oncol Lett. 2022;23(3):80. doi:10.3892/ol.2022.13200.
[8] Nel AE, Mädler L, Velegol D, et al. Understanding biophysicochemical interactions at the nano–bio interface. Nat Mater. 2009;8(7):543–557. doi:10.1038/nmat2442.
[9] Pereira M, et al. Application of light scattering techniques to nanoparticle characterization and development. Molecules. 2018;23:2998. PMCID:PMC6026678.
[10] Filippov SK, Khusnutdinov R, Murmiliuk A, et al. Dynamic light scattering and transmission electron microscopy in drug delivery: a roadmap for correct characterization of nanoparticles and interpretation of results. Mater Horiz. 2023;10(12):5354–5370. doi:10.1039/D3MH00717K.
[11] Rodriguez-Loya J, Lerma M, Gardea-Torresdey JL. Dynamic Light Scattering and Its Application to Control Nanoparticle Aggregation in Colloidal Systems: A Review. Micromachines. 2024;15(1):24. doi:10.3390/mi15010024.
[12] Pochapski DJ, Dos Santos CC, Leite GW, Pulcinelli SH, Santilli CV. Zeta potential and colloidal stability predictions for inorganic nanoparticle dispersions: effects of experimental conditions and electrokinetic models on the interpretation of results. Langmuir. 2021. doi:10.1021/acs.langmuir.1c02056.
[13] Ferro C, Florindo HF, Santos HA. Selenium nanoparticles for biomedical applications: from development and characterization to therapeutics. Adv Healthc Mater. 2021;10(16):e2100598. doi:10.1002/adhm.202100598.
[14] Han J, et al. Selenium nanoparticles: properties, preparation methods, and therapeutic applications. Chem Biol Interact. 2023;110483. doi:10.1016/j.cbi.2023.110483.
[15] Mikhailova EO. Selenium nanoparticles: green synthesis and biomedical application. Molecules. 2023;28(24):8125. doi:10.3390/molecules28248125.
[16] Zambonino MC, Quizhpe EM, Mouheb L, Rahman A, Agathos SN, Dahoumane SA. Biogenic Selenium Nanoparticles in Biomedical Sciences: Properties, Current Trends, Novel Opportunities and Emerging Challenges in Theranostic Nanomedicine. Nanomaterials. 2023;13(3):424. doi:10.3390/nano13030424.

[17] Nag S, Kar S, Mishra S, et al. Unveiling green synthesis and biomedical theranostic paradigms of selenium nanoparticles: a state-of-the-art comprehensive update. Int J Pharm. 2024;662:124535. doi:10.1016/j.ijpharm.2024.124535.
[18] Raturi P, Ahmad N, Rawat N, Singhvi N. Synthesis and biomedical based applications of selenium nanoparticles: a comprehensive review. Indian J Microbiol. 2025;65(1):204–215. doi:10.1007/s12088-024-01302-w.
[19] Vanlalveni C, Lallianrawna S, Biswas A, et al. Green synthesis of silver nanoparticles using plant extracts and their antimicrobial activities: a review of recent literature. RSC Adv. 2021;11:2804–2837. doi:10.1039/D0RA09941D.
[20] Ahmed S, Ahmad M, Swami BL, Ikram S. A review on plants extract mediated synthesis of silver nanoparticles for antimicrobial applications: a green expertise. J Adv Res. 2016;7(1):17–28. doi:10.1016/j.jare.2015.02.007.
[21] Pandey A, Lakhanpal S, Bishoyi AK, et al. Biosynthesis of silver nanoparticles from plant extracts: a comprehensive review focused on anticancer therapy. J Drug Deliv Sci Technol. 2025.
[22] Okur EE, Akdaşçi E, Eker F, Bechelany M, Karav S. Silver Nanoparticles as Anticancer Agents: Mechanisms Insight, Current Studies, and Limitations. Pharmaceuticals. 2026;19(2):241. doi:10.3390/ph19020241.
[23] Rahman M, Khatun A, Liu L, Barkla BJ. Brassicaceae Mustards: Phytochemical Constituents, Pharmacological Effects, and Mechanisms of Action against Human Disease. Int J Mol Sci. 2024;25(16):9039. doi:10.3390/ijms25169039.
[24] Glucosinolates and Omega-3 Fatty Acids from Mustard Seeds: Phytochemistry and Pharmacology. Molecules. 2022.
[25] Brand-Williams W, Cuvelier ME, Berset C. Use of a free radical method to evaluate antioxidant activity. LWT Food Sci Technol. 1995;28(1):25–30. doi:10.1016/S0023-6438(95)80008-5.
[26] Mosmann T. Rapid colorimetric assay for cellular growth and survival: application to proliferation and cytotoxicity assays. J Immunol Methods. 1983;65(1–2):55–63. doi:10.1016/0022-1759(83)90303-4.
[27] Rota C, Chignell CF, Mason RP. Evidence for free radical formation during the oxidation of 2'-7'-dichlorofluorescin to the fluorescent dye 2'-7'-dichlorofluorescein by horseradish peroxidase: possible implications for oxidative stress measurements. Free Radic Biol Med. 1999;27(7–8):873–881. doi:10.1016/S0891-5849(99)00137-9.
[28] Kalyanaraman B, Darley-Usmar V, Davies KJA, et al. Measuring reactive oxygen and nitrogen species with fluorescent probes: challenges and limitations. Free Radic Biol Med. 2012;52(1):1–6. doi:10.1016/j.freeradbiomed.2011.09.030.
[29] Lim J, Yeap SP, Che HX, Low SC. Characterization of magnetic nanoparticle by dynamic light scattering. Nanoscale Res Lett. 2013;8:381. doi:10.1186/1556-276X-8-381.
[30] Bhattacharjee S. DLS and zeta potential—what they are and what they are not? J Control Release. 2016;235:337–351. doi:10.1016/j.jconrel.2016.06.017.
[31] Pochapski DJ, Dos Santos CC, Leite GW, et al. Zeta potential and colloidal stability predictions for inorganic nanoparticle dispersions: effects of experimental conditions and electrokinetic models on the interpretation of results. Langmuir. 2021. doi:10.1021/acs.langmuir.1c02056.
[32] Monshi A, Foroughi MR, Monshi MR. Modified Scherrer Equation to Estimate More Accurately Nano-Crystallite Size Using XRD. World J Nano Sci Eng. 2012;2(3):154–160. doi:10.4236/wjnse.2012.23020.
[33] Gülçin İ. Antioxidant activity of food constituents: an overview. Arch Toxicol. 2012;86(3):345–391. doi:10.1007/s00204-011-0774-2.
[34] Monopoli MP, Åberg C, Salvati A, Dawson KA. Biomolecular coronas provide the biological identity of nanosized materials. Nat Nanotechnol. 2012;7(12):779–786. doi:10.1038/nnano.2012.207.
[35] Kopac T. Protein corona, understanding the nanoparticle-protein interactions and future perspectives: a critical review. Int J Biol Macromol. 2021;169:360–373. doi:10.1016/j.ijbiomac.2020.12.108.
[36] Akhter MH, Khalilullah H, Gupta M, et al. Impact of Protein Corona on the Biological Identity of Nanomedicine: Understanding the Fate of Nanomaterials in the Biological Milieu. Biomedicines. 2021;9(10):1496. doi:10.3390/biomedicines9101496.
[37] Samanchi S, Josthna et al. Bio Fabricated Selenium Nanoparticles and Their Therapeutic Potential: Bridging the Gap Between Elemental Selenium and Bio-Fabricated Nano Selenium. Int J Drug Deliv Technol. 2026;16(2s):408–419. DOI:10.25258/ijddt.16.408-419.
[38] Samanchi S, Josthna et al Biofabricated Sinapis nigra-Derived Selenium Nanoparticles: Physicochemical Characterization, Enhanced Antibacterial Activity, and Prospective Therapeutic Applications in Female Reproductive Health. Int J Drug Deliv Technol. 2026;16(56s).
[39] Samanchi S, Josthna et al Biofabricated Sinapis nigra-Derived Selenium Nanoparticles: Physicochemical Characterization, Enhanced Antibacterial Activity, and Prospective Therapeutic Applications in Female Reproductive Health. Int J Drug Deliv Technol. 2026;16(56s).